A DVB-S-Based Multichannel Passive Radar System for Vehicle Detection

JUNJIE LI[1], (Graduate Student Member, IEEE),
JUNKANG WEI[1], (Graduate Student Member, IEEE),
ZHIHUI CAO[1], (Graduate Student Member, IEEE),
QIN CHEN[1], (Graduate Student Member, IEEE), **LIJIE YANG**[4],
CHUNYI SONG[1,2,3], (Member, IEEE), **AND ZHIWEI XU**[1,2,3], (Senior Member, IEEE)

[1]Institute of Marine Electronic and Intelligent System, Ocean College, Zhejiang University, Zhoushan 316021, China
[2]Engineering Research Center of Oceanic Sensing Technology and Equipment, Ministry of Education, Zhoushan 316021, China
[3]Key Laboratory of Ocean Observation-Imaging Testbed of Zhejiang Province, Zhoushan 316021, China
[4]Zhejiang Lab, Hangzhou 310006, China

Corresponding author: Chunyi Song (cysong@zju.edu.cn)

ABSTRACT Vehicle detection systems play a significant role in intelligent transportation systems (ITSs). At present, vehicle detection is realized either by very costly inductive loops, by video cameras that require good weather conditions and high computing resources, or by recently developed magnetic sensors that only obtain limited detection accuracy in congested traffic conditions. To overcome these challenges, this paper develops a passive radar system that is robust to bad weather conditions, low cost and radio silent for vehicle detection. The device is installed at the side of the road under crowded traffic conditions. In the developed system, cross-correlation (CC) operation is applied to obtain suboptimal detection gain and computational complexity. To decrease the impact of interference that is independently and identically distributed (i.i.d.) across isolated frequency channels and that of the Doppler effect produced by a mobile vehicle, a multichannel joint detection scheme based on multichannel fusion (MCF) is proposed and implemented. Furthermore, to achieve high resolution, an illuminator of opportunity (IO) with wide bandwidth is selected, and the system is then designed to receive a digital video broadcast-satellite (DVB-S) signal with a bandwidth of 37.5 MHz over multiple channels simultaneously. Simulation results show that the proposed MCF achieves better performance than the single-channel-based CC, and the advantage can be enhanced by increasing the number of channels for joint detection. Field test results further verify the novelty of the MCF and the developed passive radar prototype.

INDEX TERMS Intelligent transportation systems, vehicle detection, passive radar, detection algorithms, digital video broadcasting-satellite (DVB-S), multichannel fusion.

I. INTRODUCTION

Intelligent transportation systems (ITSs) are attracting increasing attention from governments, industry and academia [1]. Vehicle detection plays a key role in ITSs. Among the popular conventional methods for vehicle detection, inductive loops are costly to install and maintain, video cameras consume high computing power [2] and do not work well under poor weather and nighttime conditions, and magnetic sensors lose detection robustness in congested traffic owing to so-called strong mutual effects [3].

In recent years, the rapid development of passive radar has been seen in air traffic and maritime target surveillance applications using various illuminators of opportunity (IOs), including FM radio [4], GSM [5], [6], DVB-T [7], [8], and DVB-S(2) [9], [10]. Among these studies, only a few works have focused on ground vehicle detection. References [6] and [8] developed a GSM-based and a DVB-T-based passive radar system for vehicle detection, respectively. To the best of the authors' knowledge, there has been no study to date examining DVB-S-based IO for vehicle detection.

The associate editor coordinating the review of this manuscript and approving it for publication was Zhenliang Zhang.

Type of IO	GSM [6]	DVB-T [7]	DVB-S [10]
Frequency	900/1800 MHz	470-840 MHz	11-12 GHz
Bandwidth	81.3 kHz	8 MHz (single channel)	37.5 MHz (single channel)
Range Resolution	1.845 km	22 m	5 m
Coverage(Typical value)	35-121 km	100 km	1500 km
Power Density $\frac{P_t G_t}{R_1^2}$	-81 dBW/m^{-2}@R_1 = 10 km	-72 dBW/m^{-2}@R_1 = 100 km	-95 dBW/m^{-2} (on earth surface)

In general, applications of passive radar strongly depend on the physical parameters of an IO, namely, the signal bandwidth, transmission power, and air volume coverage [11]. The abovementioned IO of the FM radio system could help to realize aerial target detection over a distance of hundreds of kilometers using an omnidirectional antenna at a considerable height and strong transmission power. However, due to the small bandwidth of the transmitted signal on the kHz scale, it only realizes low-range resolution. The same limitation exists in the abovementioned GSM-based passive radar for vehicle detection. A better target resolution in the bistatic range can be obtained using a DVB-T-based IO with a signal bandwidth on the MHz scale. However, it is still not enough to identify adjacent cars on crowded urban roads, which could have the minimum distance less than 10 meters. Consequently, a passive radar system with higher range resolution is required. A summary and comparison of potential IOs for vehicle detection are presented in Table1. DVB-S is selected as the IO in this work since it realizes the best range resolution among the three potential IOs.

Despite its advantage in range resolution, passive radar using DVB-S as IO still faces challenges. First, high processing gain is required to realize accurate detection for the poor power density of satellite transmitters. Directional antennas with high receiver gain and a sufficient coherent processing interval (CPI) are thus desired. However, when using a directional antenna, the fast and accurate tracing of noncooperative and fast-moving cars becomes necessary. This suggests that the detection of weak echoes needs to be accomplished within a very short interval. For instance, a regular car running at a constant speed of 120 km/h only allows a short exposure time of no more than 0.5 seconds. The short detection interval does not provide sufficient CPI, which is required to obtain substantial detection gain. Accurate antenna tuning is also difficult to achieve: an antenna horn has a pencil beam with a tiny 3 dB beamwidth of only 2.5°, which suggests that the antenna's orientation has to change frequently and precisely [12]. Second, the multipath effect might cause false alarms, particularly in urban areas. Third, the computational complexity increases dramatically with increasing observation time, i.e., taking sample intervals, owing to the high data rate of DVB-S(2).

Some passive radar systems using DVB-S as IO were developed in previous works. Single-channel-based systems have been designed for pedagogical use [9] and ISAR imaging [12]–[14]. Specifically, [13] developed a passive ISAR imaging system that was capable of simultaneously detecting

no more than two channels of DVB-S(2), but the test results were not demonstrated by applying multichannel joint detection. References [12] and [14] developed a system using both DVB-T and DVB-S as IOs, but again, they were only capable of simultaneously detecting no more than two channels of DVB-S. Under the scenario of mobile target detection, a cross-ambiguous function may achieve optimal detection performance [15]. However, this is not the desired choice for implementation owing to its high computational complexity [16]. [17] proposed a noncoherent fusion for detection results obtained by different IOs over frequency channels occupying different bandwidths. A multiple-channel joint detection strategy was developed in our previous work [26], in which fusion weights were determined according to the status of surveillance channels under time-varying interference. The method not only mitigated the impact of the Doppler effect by decreasing the observation time but also improved robustness to interference that was independently and identically distributed (i.i.d.) over isolated frequency channels. To the best of our knowledge, no work has developed a passive radar prototype for the IO of DVB-S with the capability of performing detection over three isolated channels of the same bandwidth jointly and achieving a detection decision based on weighted fusion.

As the extended works of [26], this paper develops a prototype by implementing the algorithm proposed in [26] and verifies the performance through more comprehensive simulation studies and field test results of vehicle detection. The main contributions of this paper are summarized as follows:

1) The algorithm proposed in [26] is based on multi-channel fusion (MCF). To further improve its robustness, a new module called batch normalization (BN) is applied prior to the fusion operation to address the inconsistency of amplitude (IA) among the multiple frequency channels. More comprehensive simulations are then performed to further understand and verify the performance of the MCF-based detection method.

2) A system prototype with MCF implementation has been well developed, and the field test results verify that the proposed MCF solution can successfully detect the static/mobile vehicles and achieve better detection performance than the technique using CC.

The rest of the paper is organized as follows. In Section II, the problem of weak echo wave detection is formulated. In Section III, the MCF-based algorithm is presented and analyzed. The design and field test results of implementation

TABLE 2. Input value of (1) and (2).

Symbol	Quantity	Value
σ	RCS of Target	10 dBsm
G_R	Receiver antenna gain	34 dB
$P_T G_T$	Transmitter ERIP	56 dBW
f_0	Carrier frequency	12 GHz
R_T	Transmitter range	36979.1 km
T_c	Coherent processing interval	0.1 s
T	Noise temperature	270 K
B_N	Noise bandwidth	40 MHz
B_S	Signal bandwidth	40 MHz
G_p	Integration gain	65 dB
c	Velocity of light	3×10^8 m/s
k	Boltzmann's constant	$1.38 \times 10^{-23} J/K$
L_s	System loss	5 dB

system prototype are demonstrated in Section IV. Finally, conclusions are drawn in Section V.

II. PROBLEM FORMULATION

This section formulates the problem of detecting weak echo waves from moving targets. The challenge of weak echo wave detection using the IO of DVB-S is demonstrated first, and the performance limitations of single-channel detection are then discussed.

A. WEAK ECHO WAVE OF SATELLITE-BASED IO

The performance of a passive radar is usually analyzed using the well-known bistatic radar equation [11]. The receiving power of the echo wave based on the IO of DVB-S can then be calculated by:

$$S = \frac{P_T G_T G_R c^2 \sigma L_s}{(4\pi)^3 f_0^2 R_T^2 R_R^2} \quad (1)$$

The definitions of symbols and their values in the case of Apstat-6C 134°E [19] are listed in Table2. R_R is the range between the target and the receiver. The input signal-to-noise ratio (SNR) [16], which is denoted as the SNR of the received echo wave, is given by

$$SNR_I = \frac{S}{N_s} \quad (2)$$

where $N_s = kB_N T$, is the noise power of receiving system. The output SNR of the echo wave after coherent signal processing in the passive radar is then denoted as

$$SNR_O = SNR_I G_p \quad (3)$$

where $G_p = B_S T_c$, is the coherent integration gain. Fig. 1 shows the curve of the input/output SNR of the echo wave versus range when setting the required output SNR to 10 dB, which is obtained by setting CPI to 0.1 seconds. In real applications, the input SNR might be even lower due to additional losses [20] and high radar cross-section (RCS) sensitivity in the Ku-band [14]. Obviously, the basic challenge of DVB-S based passive radar is the low SNR of received weak echo wave.
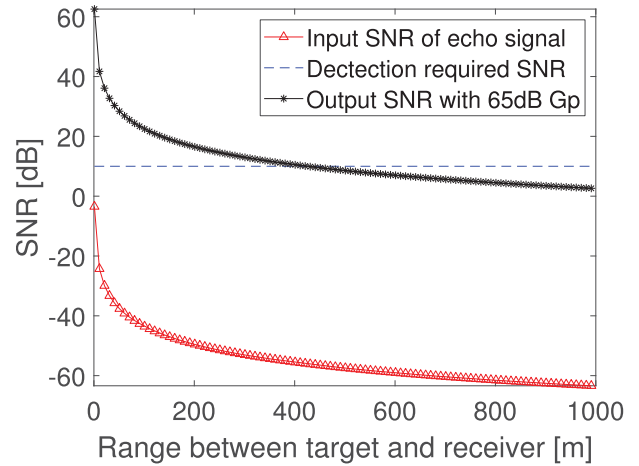

FIGURE 1. The input/output SNR of the echo wave versus range between the target and receiver.

B. LIMITATION OF SINGLE-CHANNEL-BASED DETECTOR

For a passive bistatic radar system with $M(M \geqslant 1)$ channels, both the reference signal and reflected signal are received. The reference signal of the m-th channel is given by

$$S_{ref,m}(n) = a_{ref,m}s_m(n) + v_{ref,m}(n) \quad (4)$$

where $m = 1, 2, 3, \ldots M$, and M is the number of channels; $n = 1, 2, 3, \ldots, N$ and N is the number of samples in each channel; $S_{ref,m}$ is reference signal from the m-th reference channel (RC); $a_{ref,m}$ is the strength of reference signal in the m-th RC; $s_m(n)$ can be view as random variable of transmitted signals from satellite in the m-th RC; and $v_{ref,m}(n)$ is noise over the channel and it is supposed to follow complex Gaussian distribution with zero mean and variance of $\sigma_{ref,m}^2$, i.e., $v_{ref,m}(n) \sim \mathcal{CN}(0, \sigma_{ref,m}^2)$.

The reflected signal in the m-th surveillance channel (SC) is denoted as $S_{surv,m}(n)$, which is always the combination of direct path interference (DPI), signal reflected from the target of interest and noise, i.e.

$$S_{surv,m}(n) = a_{dpi,m}s_m(n) + a_{surv,m}s_m(n - \tau) \\ \times e^{j2\pi f_d t} + v_{surv,m}(n) \quad (5)$$

where $a_{dpi,m}$ stands for the strength of the DPI, which is the leakage of the direct path signal due to imperfect antenna directivity; $a_{surv,m}$ is the strength of the echo signal in the m-th SC, τ is the arrival delay of target echo compared to the reference signal, f_d is the Doppler shift caused by the mobile target; and $v_{surv,m}(n)$ is noise in the m-th SC following complex Gaussian distribution with zero mean and variance of $\sigma_{surv,m}^2$, i.e., $v_{surv,m}(n) \sim \mathcal{CN}(0, \sigma_{surv,m}^2)$.

The problem of detecting the existence of a target is then formulated as a binary hypothesis, as

$$H_0 : S_{surv,m}(n) = a_{dpi,m}s_m(n) + v_{surv,m}(n)$$
$$H_1 : S_{surv,m}(n) = a_{dpi,m}s_m(n) + a_{surv,m}s_m(n - \tau)$$
$$\times e^{j2\pi f_d t} + v_{surv,m}(n) \quad (6)$$

where H_0 and H_1 represent the absence and presence of the target of interest, respectively.

If DPI is efficiently suppressed using the least mean squares (LMS) and recursive least squares (RLS) algorithm [21], the detection problem can be simplified as:

$$H_0 : S_{surv,m}(n) = v_{surv,m}(n)$$
$$H_1 : S_{surv,m}(n) = a_{surv,m}s_m(n - \tau)e^{j2\pi f_d t} + v_{surv,m}(n) \quad (7)$$

Without losing generality, we assume that $v_{ref,m}(n)$ and $v_{surv,m}(n)$ are time-varying over each channel and i.i.d. across isolated frequency channels. The distribution of $\sigma^2_{surv,m}$ is given by

$$\sigma^2_{surv,m} = K_m \sigma^2_{surv} \quad (8)$$

where σ^2_{surv} is an expected noise variance, K_m is a fluctuation factor following log-normal distribution, as

$$10 \log_{10} K_m \sim N\left(0, \sigma^2_K\right) \quad (9)$$

where σ^2_K denotes the fluctuation coefficient. Related work on modeling multichannel fluctuations can be found in [22].

A passive radar then makes a decision following

$$T = T(S_{ref}, S_{surv}, N) \underset{H_0}{\overset{H_1}{\gtrless}} \bar{\lambda} \quad (10)$$

where $\bar{\lambda}$ is the decision threshold, and T denotes a generalized decision statistic.

When using the single-channel-based CC detector, the decision statistic is given by

$$T_{CC,m}(\tau) = \frac{1}{N_{CC}} \left| \sum_{n=1}^{N_{CC}} S^*_{ref,m}(n)S_{surv,m}(n - \tau) \right|^2 \quad (11)$$

where N_{CC} is the length of signal and also suggests the coherent detection interval.

According to the above analysis results, the time-varying interference leads to unstable and degraded detection performance based on a single specific channel. In addition, the Doppler frequency shift f_d deteriorates the coherence. The required long CPI by single-channel-based detection will then significantly degrade the detection performance. To overcome these challenges, a multichannel-based detection algorithm is proposed in the next section.

III. MCF-BASED ALGORITHM

This section illustrates the proposed MCF-based detection algorithm, which decreases the coherent integration time by dividing the operation over a single channel into parallel and joint operations in multiple channels, and as a result, the impact of the Doppler effect on the detection performance is mitigated. Moreover, interference usually lasts for a period that is much longer than a detection period, and MCF-based detection can effectively smooth the interference that follows i.i.d. over isolated frequency channels. In this section, the structure of MCF is first illustrated. The performance of the proposed MCF is then evaluated by simulation.

A. STRUCTURE OF MCF

In this section, we illustrate the structure of the proposed MCF. Based on the model of the passive radar system discussed above, MCF is capable of performing multichannel joint detection, and its decision statistic is given by

$$T_{\text{MCF}}(\tau) = \frac{1}{MN} \left| \sum_{m=1}^{M} W_m \sum_{n=1}^{N} t_m(\tau) \right|^2 \quad (12)$$

where W_m is the weight for the test results obtained from the m-th channel and used for the fusion operation, and $t_m(\tau)$ is denoted as

$$t_m(\tau) = S^*_{ref,m}(n)S_{surv,m}(n - \tau) \quad (13)$$

The MCF-based detector receives intermediate frequency (IF) signals simultaneously from multiple channels and outputs the fusion result. Its structure is shown in Fig. 2, which shows that the detector mainly consists of a data preprocessor, Fast cross-correlation (Fast-CC) and fusion center. The details are then discussed below.
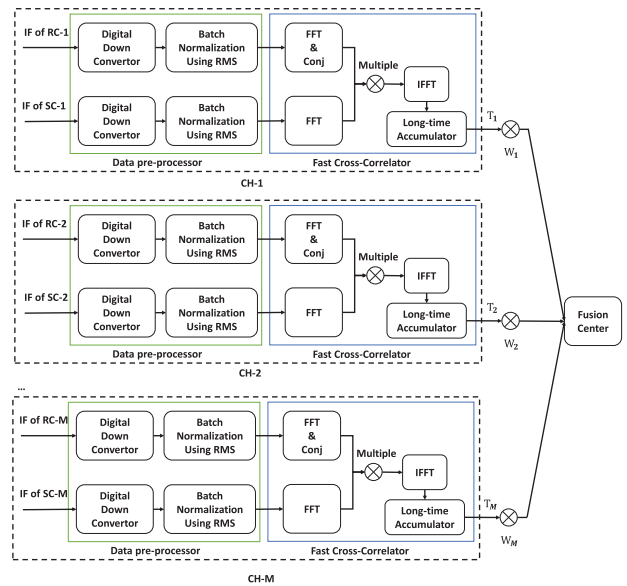

FIGURE 2. Structure of MCF.

1) DATA PREPROCESSING
As shown in Fig. 3, $a_{ref,m}$ and $a_{surv,m}$ may vary among different frequency channels during a detection period. This is the so-called IA, which will result in different scales of CC outputs over different channels and therefore degrade fusion performance. Herein, we propose data preprocessing called batch normalization (BN) to address this problem. The IF signals are first digitally downconverted (DDC) to complex baseband and are then processed by BN. The processing steps of BN are introduced below.
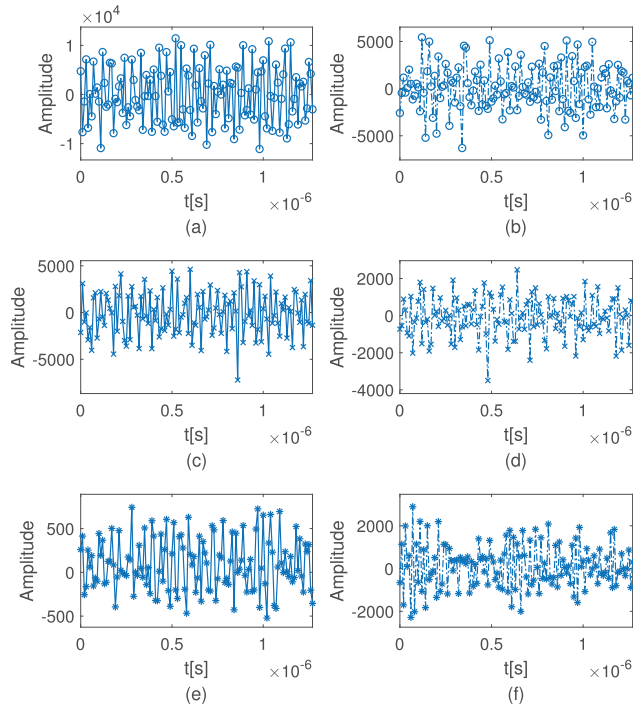
FIGURE 3. IA of reference and surveillance IF signal: (a) reference IF of CH1; (b) surveillance IF of CH1; (c) reference IF of CH2; (d) surveillance IF of CH2; (e) reference IF of CH3; (f) surveillance IF of CH3. (without BN). Definition of CH1-3 see Table 4 (in Section IV-A).

The $\hat{a}_{ref,m}$ and $\hat{a}_{surv,m}$ are first estimated by applying the root-mean-square (RMS) algorithm [23] as

$$\begin{cases} \hat{a}_{ref,m} = \text{RMS}\left[S_{ref,m}(n)\right] \\ \hat{a}_{surv,m} = \text{RMS}\left[S_{surv,m}(n-\tau)\right] \end{cases} \quad (14)$$

The $t_m(\tau)$ defined in (13) is then normalized, as

$$\overline{t_m(\tau)} = \frac{t_m(\tau)}{\hat{a}_{ref,m}\hat{a}_{surv,m}} \quad (15)$$

The decision statistic of MCF in (12) can then be modified, as

$$T_{\text{MCF}}(\tau) = \frac{1}{MN}\left|\sum_{m=1}^{M} W_m \sum_{n=1}^{N} \overline{t_m(\tau)}\right|^2 \quad (16)$$

where $\sum_{n=1}^{N} \overline{t_m(\tau)}$ is denoted as the normalized CC output.

2) FAST CROSS-CORRELATOR
The computation complexity of the $\sum_{n=1}^{N} \overline{t_m(n)}$ is $O(N^2)$ and is time-consuming in the time domain [24]. Fast-CC is then adopted to accelerate the computation of CC operation by transforming the operations to the frequency domain as

$$\sum_{i=1}^{N} \overline{t_m(n)} = \frac{F^{-1}\left\{F^*\left[S_{ref,m}(n)\right]F\left[S_{surv,m}(n-\tau)\right]\right\}}{\hat{a}_{ref,m}\hat{a}_{surv,m}} \quad (17)$$

where $F(x)$ denotes the fast Fourier transform (FFT), $F^{-1}(x)$ denotes its inverse fast Fourier transform (IFFT), and

"*" denotes the complex conjugate. By applying Fast-CC, the complexity of CC is reduced to $O(N\log(N))$.

3) FUSION CENTER AND WEIGHT DESIGN
The multichannel fusion weights defined in (12) are determined at the fusion center. A linear fusion method that determines the weight for passive multistatic radar was developed with the closed form of its optimization [25]. However, this method is hard to implement since it requires an accurate estimation of two parameters: the variance and mean of the decision statistic under H_0 and H_1. Our previous work in [26] developed a strategy that is better for applications with sub-optimal performance as

$$W_m = \frac{1/\hat{\sigma}_{surv,m}}{\sum_{m=1}^{M} 1/\hat{\sigma}_{surv,m}} \quad (18)$$

and

$$\hat{\sigma}_{surv,m}^2 = \frac{\left(\mathbf{S}_{surv,m} - \bar{S}_{surv,m}\right)^T \left(\mathbf{S}_{surv,m} - \bar{S}_{surv,m}\right)}{N} \quad (19)$$

where $\mathbf{S}_{surv,m}$ denotes the vector form of $S_{surv,m}(n)$ and $\bar{S}_{surv,m}$ denotes the mean of $S_{surv,m}(n)$; $\hat{\sigma}_{surv,m}^2$ is the estimation of noise power variance for m-th SC.

The proposed weight of our strategy is close to the optimal weight when only the variety of $\sigma_{sruv,m}$ is taken into account. That is, we assume $v_{ref,m}$ and DPI are ignoring, and assume $a_{ref,m}$ and $a_{surv,m}$ are well estimated.

B. NUMERICAL ANALYSIS
In this section, Monte Carlo simulations are performed to evaluate the performance of the proposed MCF scheme. The simulated signals are generated according to the standard document of DVB-S [27]. Based on the assumption that the varying interference is quasi-static over several consecutive detection durations in one channel and follows i.i.d. across frequency channels, the expected input SNRs of the echo wave and reference signal are respectively given by

$$\text{SNR}_{SC} = 10\log_{10}\frac{|a_{surv}|^2}{\sigma_{surv}^2} \quad (20)$$

$$\text{SNR}_{RC} = 10\log_{10}\frac{|a_{ref}|^2}{\sigma_{ref}^2} \quad (21)$$

In the simulations, σ_K^2 is set to 10 for quantifying the variance of channels. Considering the challenge in practice that the received echo signals could be with extremely low SNR, the expected SNR_{SC} is set between -72 and -32 dB, and a large value of CPI is then applied in the simulation to obtain significant processing gain. The total CPI is set the same for different detectors, i.e., $N_{CC} = N_{MCF} = N_{LF} = MN$. By setting the sample rate $f_s = 100$ MHz, then $MN = 3.84 \times 10^7$, which is equivalent to 0.384 seconds. The delay of echo target $\tau = 30$ bin, and the probability of false alarm $P_{fa} = 10^{-2}$. The decision threshold that achieves the specific P_{fa} is determined empirically based on the 10^3 trials under H_0. The detection probability (P_d) is then calculated based on another 10^3 trials

TABLE 3. The parameters of simulation setting.

Symbol	Parameter	Value
σ_K^2	Variance of channel	10
f_d	Interest Doppler frequency shift	3 Hz
τ	Target delay	30 bin
f_s	Sample rate	100 MHz
N_{CC}	CPI of CC	3.84×10^7
N_{MCF}	CPI of MCF	3.84×10^7
N_{LF}	CPI of LF	3.84×10^7
M	Channel number of MCF and LF	3
SNR_{RC}	Expected input SNR of RC	15 dB
SNR_{SC}	Expected input SNR of SC	[-72:-32] dB
P_{fa}	False alarm rate	10^{-2}
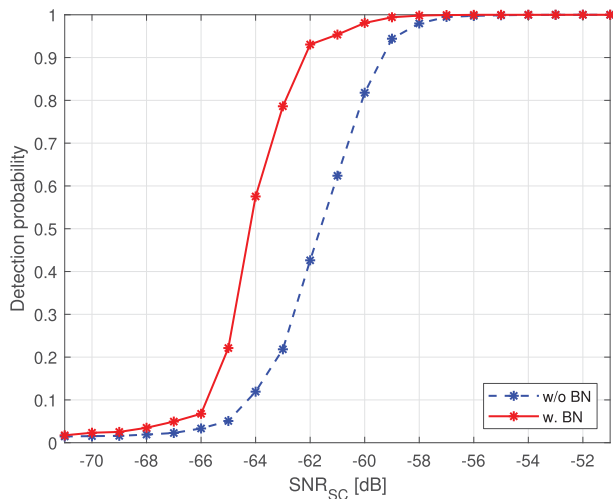
FIGURE 4. Performance of MCF ($M = 3$) with and without applying data preprocessing (BN).
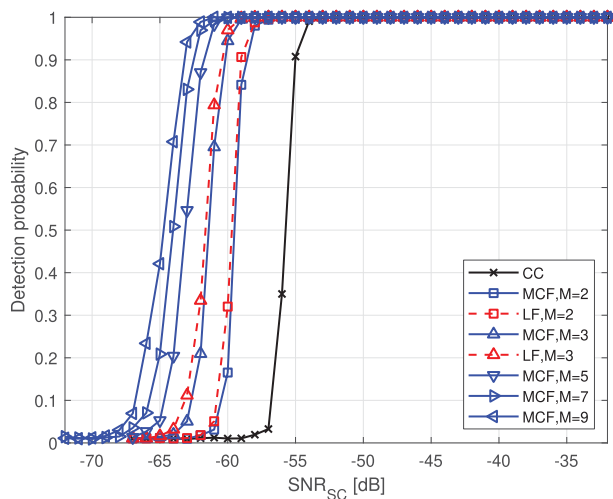

FIGURE 5. P_d versus SNR_{SC} when only the varying interference is considered.

under H_1 for each expected SNR_{SC}. The main simulation parameters are summarized in Table 3.

The performance gain by applying the BN operation defined in (14) and (15) is first evaluated. The comparison results are demonstrated in Fig. 4 for the two cases with
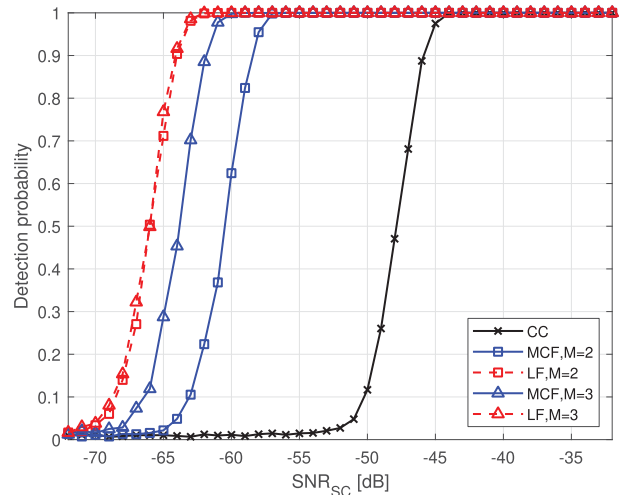

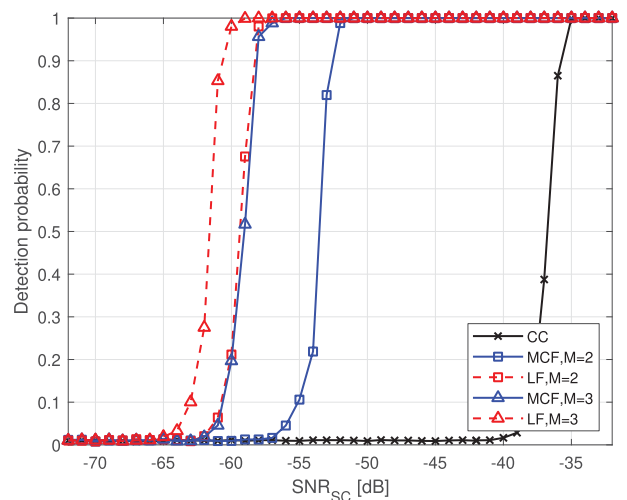**FIGURE 6.** P_d versus SNR_{SC} when only the Doppler frequency shifting is considered.

FIGURE 7. P_d versus SNR_{SC} when both the Doppler frequency shifting and varying interference are considered.

applying BN and without applying BN, with setting the channel number M = 3. The comparison results verify that the data preprocessing of BN has improved the performance of MCF.

Considering that the weight design, i.e., the fusion strategy, is one of the key characteristics in the MCF, the linear fusion (LF) [25] is chosen as the optimal baseline scheme for performance comparison. The LF was originally developed for multistatic passive radar. The fusion strategy could also be extended for the multichannel joint detection. The LF applies the full prior information of reference channel status and surveillance channel status, i.e. a_{ref}, a_{surv}, σ_{ref} and σ_{surv} defined in (4) and (5), respectively, in the fusion. Therefore, the LF also serves as the benchmark of the optimal performance in the presence of time-varying interference and Doppler shift.

Fig. 5 demonstrates the performance of the CC in (11), the proposed MCF in (16) and the LF when only the effect
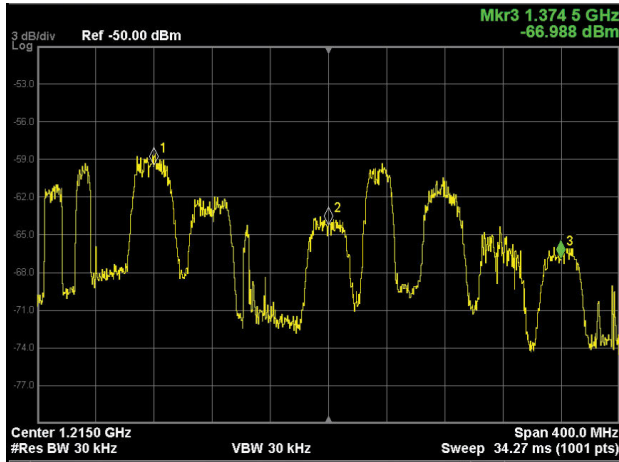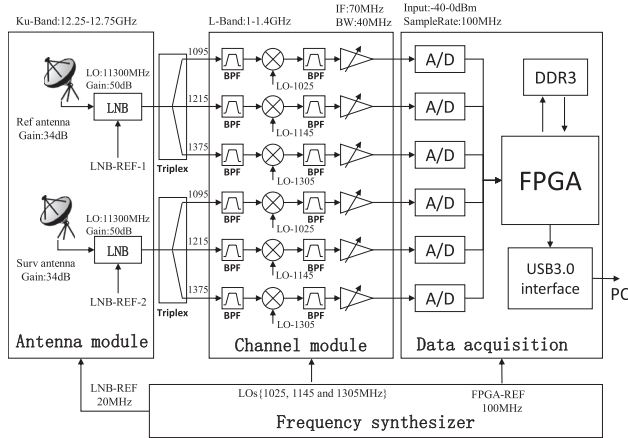
FIGURE 8. MCPC property of Apstar-6C.

FIGURE 9. The diagram of implementation system.

of time-varying interference is considered. Among the three schemes, the MCF achieves better performance than the CC, and the LF achieves the best performance. Moreover, the performance of the MCF improves with the increase of M; as a result, the advantage of the MCF over the CC could be enhanced by increasing M. We also notice an interesting result where the detection gain obtained by increasing M from 2 to 3 approximates to that obtained by increasing M from 3 to 5 and also approximates to that obtained by increasing M from 5 to 9.

A performance comparison is then made by only considering the effect of the Doppler frequency shift. The results in Fig. 6 show that the performance advantage obtained by the MCF ($M = 2$) over the CC is significantly larger than the advantage obtained by the MCF ($M = 3$) over the MCF ($M = 2$). The comparison results suggest that the MCF ($M = 2$) can efficiently mitigate the effect of Doppler frequency offset and obtain significant detection gain by reducing the CPI over each frequency channel. However, the detection performance is only slightly increased when further increasing the value of M.
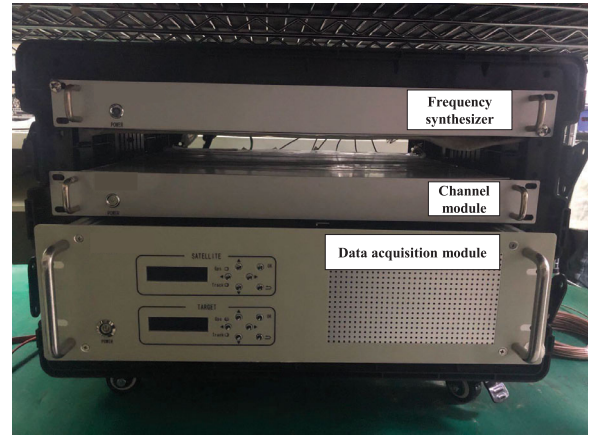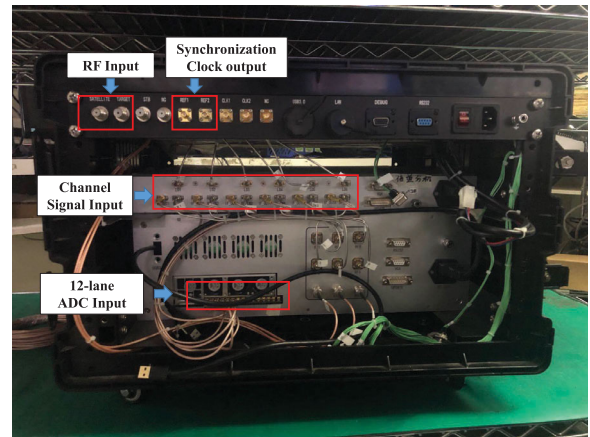
FIGURE 10. Implementation prototype with frequency synthesizer, channel module and data acquisition module: (a) front-end; (b) back-end.
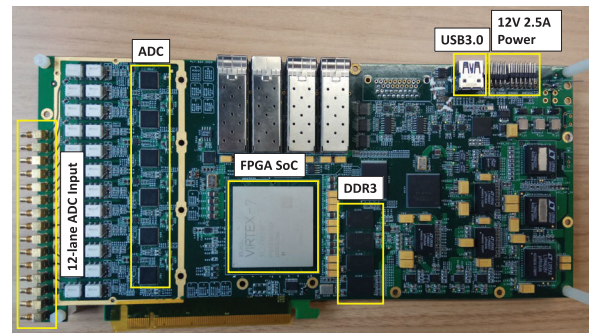

FIGURE 11. Data acquisition board.

In Fig. 7, the performance comparison results are demonstrated by considering the impacts of both the Doppler frequency shift and the time-varying interference. The comparison results in Fig. 5 and Fig. 6 show that the performance advantage obtained by the MCF over the CC is more significant.

IV. IMPLEMENTATION SYSTEM AND FIELD TEST
To further verify the effectiveness of the proposed MCF algorithm, an implementation system prototype is developed,
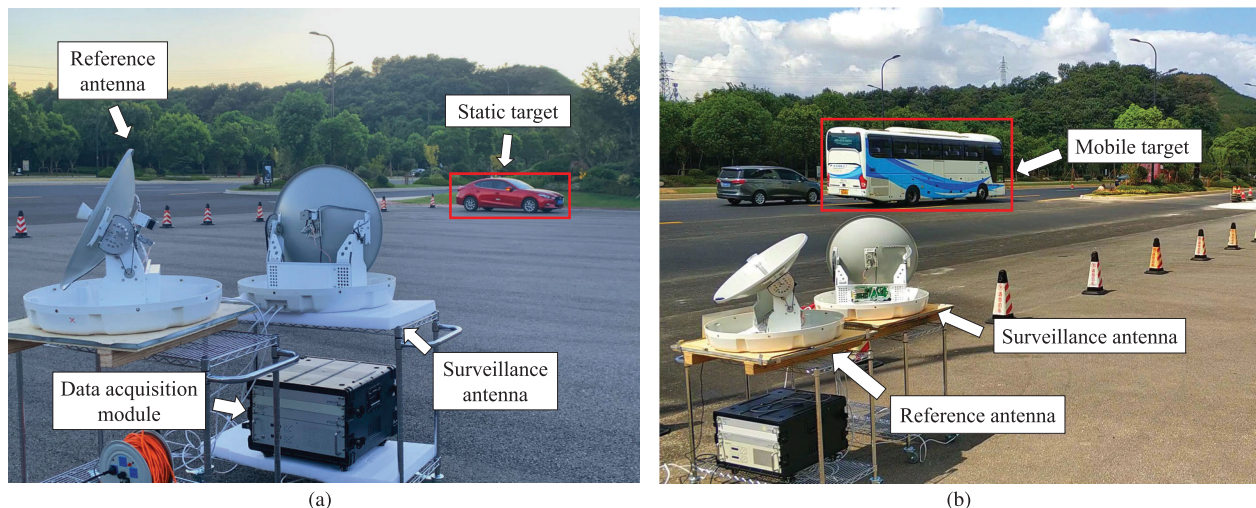
FIGURE 12. Experimental set-up for vehicle detection. (a) detection for the ST; (b) detection for the MT.

and field experiments are performed at the roadside of an urban highway located in Zhoushan city, China.

A. IMPLEMENTATION SYSTEM

The implementation system is designed based on a characteristic called multiple channel per carrier (MCPC), which is a common form of satellite transmission. In MCPC, a single carrier is utilized to transmit multiple channels. That is, multiple video or audio channels are transmitted over a single carrier by utilizing time division multiplexing (TDM), and multiple channels are multiplexed together for a single radio frequency (RF) carrier. The multiple channels can therefore be downshifted to a desired IF by well-designed local oscillators (LOs) and captured by a bandpass filter (BPF). As a result, the information transmission efficiency can be improved.

However, the fusion of information from multiple channels with different bandwidths can impose many difficulties on both signal processing and hardware implementation; in addition, the detection range resolution largely depends on the signal bandwidth of the IO. We then summarize some guidelines for selecting the IO of satellites and channels as follows: 1) the IO (i.e., satellite) should cover the surveillance area of interest; 2) the IO should provide multiple channels of the same bandwidth; 3) frequencies of the selected channels should be isolated to increase the possibility that the received interference is i.i.d. across frequency channels.

The Apstar-6C satellite basically meets all of the above requirements. The MCPC property of Apstar-6C is displayed in Fig. 8. Based on the 3rd rule, the three channels with IF equal to 1.095, 1.215 and 1.375 GHz are selected [19] and called CH1, CH2 and CH3, respectively. The specific channel information for MCPC in Apstar-6C is summarized in Table 4.

As shown in Fig. 9, the system prototype consists of antenna module, frequency synthesizer, channel module and data acquisition board.

TABLE 4. Summary of MCPC in Apstar-6C.

No. of Channel	IF(after LNB)/GHz	Bw/MHz	PSD/dBm/Hz
1 (CH1)	1.095	37.5	-105
2	1.135	37.5	-109
3 (CH2)	1.215	37.5	-110
4	1.295	37.5	-108
5 (CH3)	1.375	37.5	-115

1) ANTENNA MODULE

The antenna module consists of two identical commercial horn antennas and a low-noise-block (LNB). One antenna is used for surveillance, and the other is used for reference. The surveillance antenna tracks the target, while the reference antenna points to the IO of the Apstar-6C satellite. Each antenna provides 34 dB gain with a diameter of 60 cm. Moreover, each antenna is equipped with a GPS/IMU unit to obtain precise information about the location and antenna pointing direction. In particular, the surveillance antenna is also equipped with a laser pointer, which helps to identify the antenna direction visually. Based on the design, both antennas enable two-axis stable three-axis tracking and azimuth 360° continuous tracking. The adjustment range of the elevation angle is 0-90°, and the tracking polarization angle ranges from $-90°$ to $+90°$. LNB is used as the first-stage downconverter, shifting RF signals from the Ku-band into the lower L-band (1.0-1.4 GHz) and amplifying them with 50 dB gain as well.

2) FREQUENCY SYNTHESIZER

The frequency synthesizer (FS) realizes the LNB-REF that ensures coherent operation of LNB with the rest of the system. It also produces three LOs at frequencies of 1025, 1145 and 1305 MHz for the channel module. The FS also generates a reference clock for the signal acquisition module.

3) CHANNEL MODULE

The channel module (CM) acts as a second-stage downconverter, which is capable of working in parallel among

FIGURE 13. Range-Doppler mappings of echo wave when detecting the ST. (a) CH1; (b) CH2; (c) CH3.
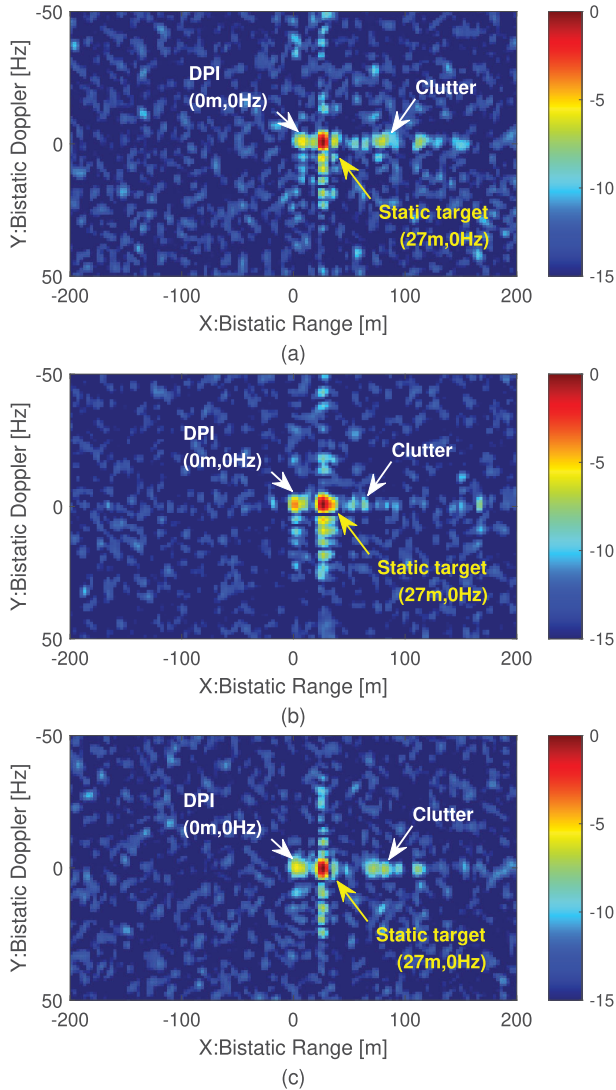

FIGURE 14. Range-Doppler mappings of echo wave when detecting the MT. (a) CH1; (b) CH2; (c) CH3.

different frequency bands. Specifically, the CM splits and purifies L-band signals from triplex into IF multiband signals. The expected level of the reference signal is approximately −110 dBm at the antenna. To avoid interference caused by adjacent channel leakage, a triplex in the form of a cavity resonator is designed and used to achieve >60 dBc isolation between adjacent channels. Combined with the FS, the CM converts the frequency of L-band signals to the same IF band of 70 MHz. Designating the bandwidth of the BPF as 40 MHz, the CM then outputs six-way signals, among which three are CH1, CH2 and CH3 for the reference and the other three are CH1, CH2 and CH3 for surveillance. The hardware of the implementation system including CM and FS is shown in Fig. 10.

4) DATA ACQUISITION MODULE
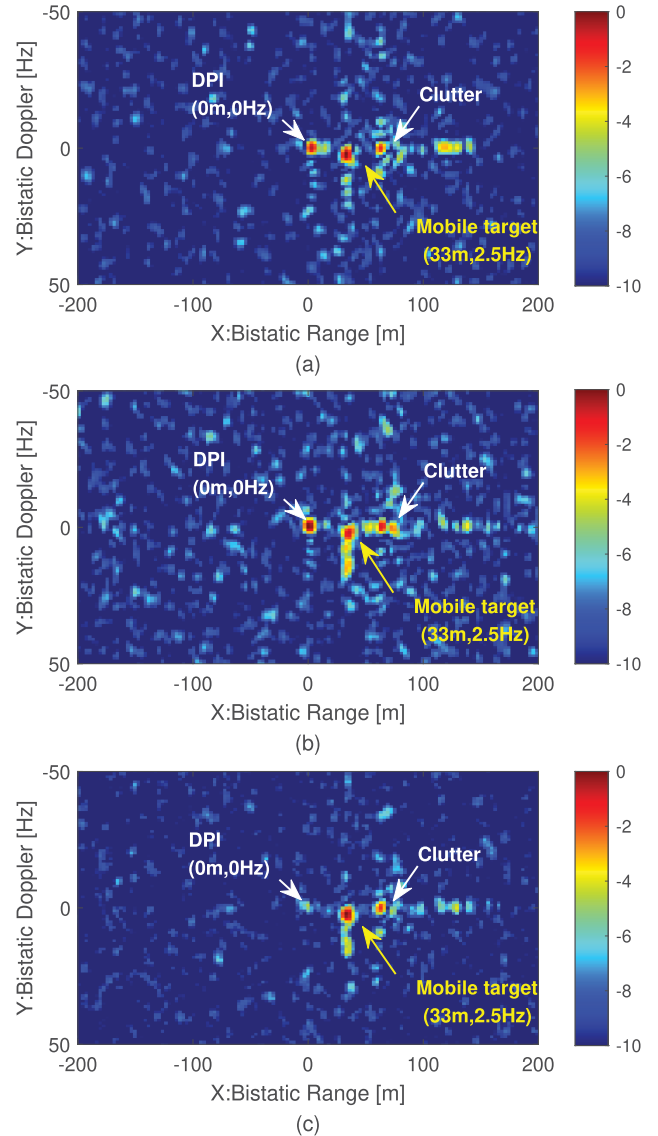The data acquisition module is designed to digitize the IF signals and then transfer them to a personal computer (PC)

for postprocessing. The hardware of the data acquisition board is shown in Fig. 11. It mainly consists of six-path RF interfaces, six ADCs, an FPGA-based master control unit and a USB 3.0 interface. The IF signals of 70 MHz are first sampled by a 16-bit ADC (AD9650-105EBZ) at a sample rate of 105 Msps. HMC7043 is then used to achieve the synchronization of multiple ADC inputs by splitting six clocks into different ADCs. This realizes a latency below 10 ms. The FPGA chip (XC7VX690T-2FFG1761) processes the sampled data and transfers them to DDR3 SDRAM for temporary storage. The USB3.0 interface chip (CYUSB3014) provides a slave FIFO mode to realize duplex communication between the FPGA and PC and obtains data rate of 3.2 Gbps in real measurements. This solution enables the signal acquisition module to transfer the IF signals of six channels to a high-performance PC for further postprocessing.
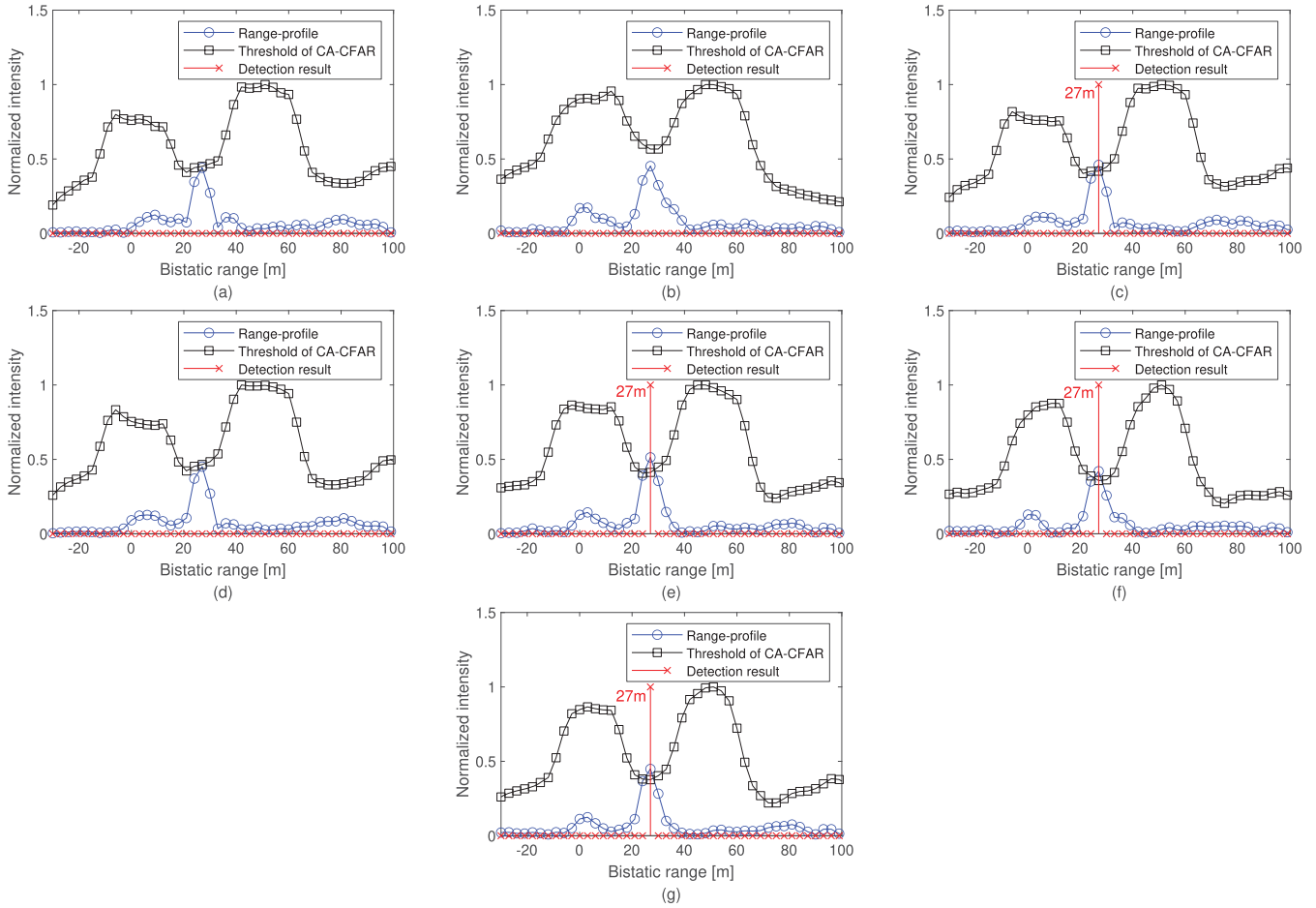
FIGURE 15. Range profiles, thresholds and detection results for the ST: (a) CC (CH1); (b) CC (CH2); (c) CC (CH3); (d) MCF (M = 2, CH1&CH2); (e) MCF (M = 2, CH1&CH3); (f) MCF (M = 2, CH2&CH3); (g) MCF (M = 3).

5) POSTPROCESSING UNIT
The postprocessing unit consists of a high-performance PC with Core i7-8750H and SSD. It is implemented with BN, Fast-CC and weight fusion and achieves detection results based on the data from the data acquisition module.

B. FIELD TESTS
In this section, the feasibility of vehicle detection using the IO of DVB-S is verified, and the performance of the proposed MCF is evaluated by field tests, with one for the detection of the noncooperative static target (ST) and one for the noncooperative mobile target (MT). The test is conducted at Zheda Road, a highway located to the east of Zhoushan Campus of Zhejiang University, with latitude and longitude of approximately 122.2° and 30°, respectively. The detection scenes are shown in Fig. 12: the ST of interest is a car, and the MT of interest is a bus. The speed limit on Zheda Road is 80 km per hour. In the detection, the reference antenna is pointing at the Apstar-6C (IO), while the surveillance antenna is pointing at the target of interest.

The theoretical values of bistatic range D and bistatic Doppler shift f_d are respectively given by [18]

$$D = |\vec{r}_1| + |\vec{r}_2 - \vec{r}_0| \quad (22)$$
$$f_d = \frac{1}{\lambda} \left[\frac{\vec{r}_2 \cdot \vec{v}}{|\vec{r}_2|} + \frac{\vec{r}_1 \cdot \vec{v}}{|\vec{r}_1|} \right] \quad (23)$$

where $\vec{r}_1$ is the vector from the GEO satellite to target, $\vec{r}_2$ is the vector from target to receiver, $\vec{r}_0$ is the vector from the GEO satellite to the receiver, $\vec{v}$ is the target velocity vector, λ is the length of wave in RF. The expected velocity of the target ranges between 40 and 60 km/h.

To minimize the effect of the Doppler shift, the surveillance location and orientation of the surveillance antenna need to be first determined. The direction of the surveillance antenna is fixed to a specific area. Once vehicles of interest pass through this area, the reflected DVB-S signals are then recorded. By doing this, the Doppler shift produced by noncooperative vehicles is mitigated. The experimental scenario is shown in Fig. 12(b).

A passenger bus is selected as the target to be detected and its physical specification can be summarized as:
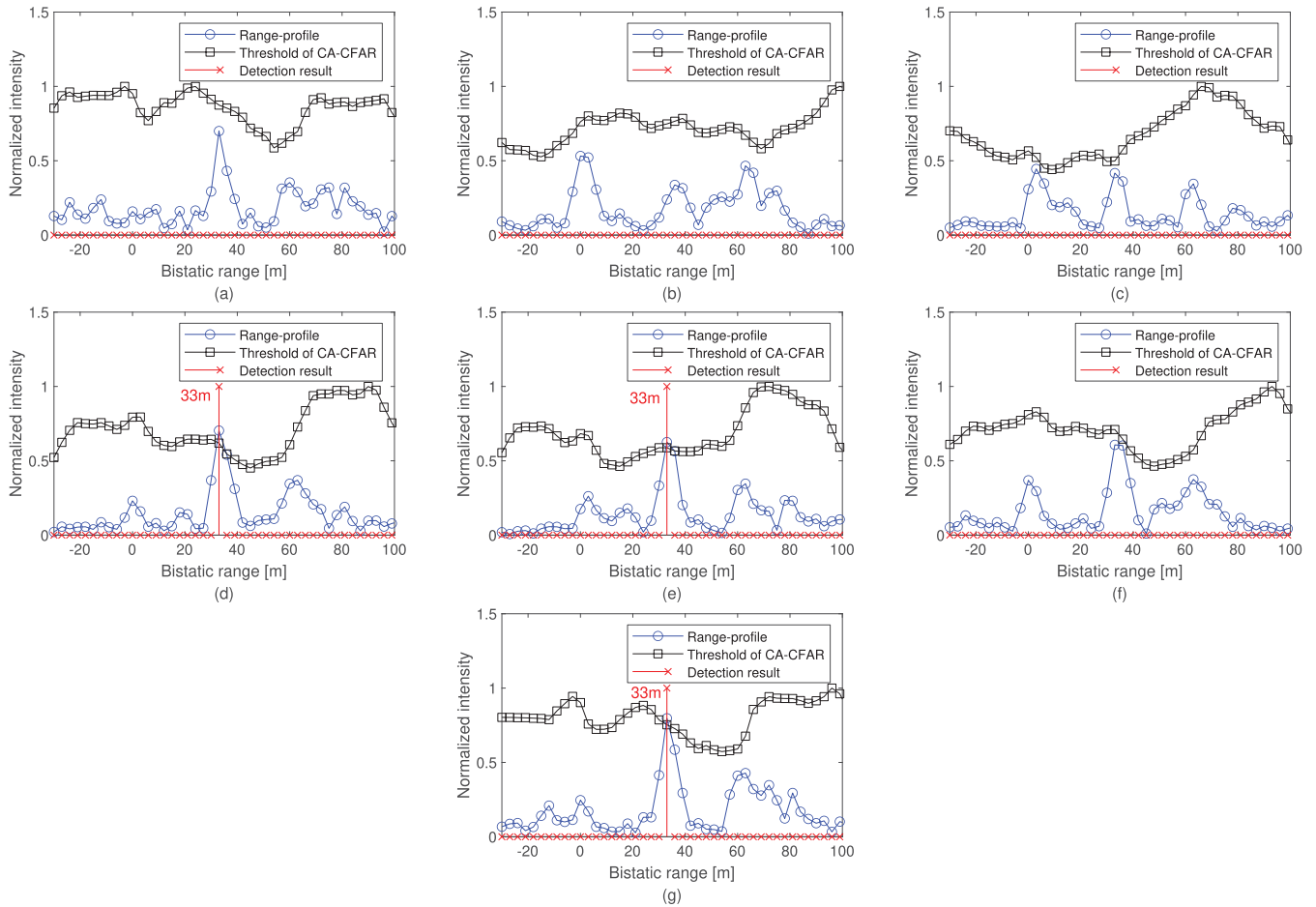
FIGURE 16. Range profiles, thresholds and detection results for the MT: (a) CC (CH1); (b) CC (CH2); (c) CC (CH3); (d) MCF (M = 2, CH1&CH2); (e) MCF (M = 2, CH1&CH3); (f) MCF (M = 2, CH2&CH3); (g) MCF (M = 3).

- Length: 11.4 m
- Width: 2.5 m
- Height: 3.8 m

To understand the ground truth of the target's parameters of interest, i.e., D and f_d, range-Doppler mapping (RDM) [18] is produced, and the results are shown in Fig. 13 and Fig. 14 for the ST and MT, respectively. In Fig. 13, the RDMs of CH1, CH2 and CH3 demonstrate good coincidence in terms of the DPI (0 m, 0 Hz), target echo (27 m, 0 Hz) and ground clutter (63 m, 0 Hz). The target peak is visible at 27 m with a value approximately 10 dB above the disturbance power level. The results in Fig. 14 also show good coincidence among the three channels in terms of the DPI (0 m, 0 Hz), target echo (33 m, 2.5 Hz) and ground clutter (63 m, 0 Hz).

Considering the difficulty of obtaining detection threshold according to the Neyman-Pearson (NP) rule under complex clutter, the cell averaging constant false alarm rate (CA-CFAR) [28] detector is applied to achieve the detection results based on the range profiles for the MCF and the CC, respectively. The parameters of CA-CFAR are set as follows: the reference cell $N_r = 20$ and guard cell $N_g = 6$. The probability of false alarm is fixed to 10^{-3}.

The detections are performed over the three channels, CH1, CH2 and CH3. The MCF ($M = 2$) can then be performed over three combinations of channels: CH1&CH2, CH1&CH3 and CH2&CH3. The detection results are shown in Fig. 15 and Fig. 16, which consist of the detection results of CC over each of the three channels, the detection results of MCF ($M = 2$) over the three combinations of two channels, and the detection results of MCF ($M = 3$).

The detection results for the ST are shown in Fig. 15. The conventional CC has successfully detected the target only over CH3 and has failed to detect the target over the other two channels. By contrast, the MCF ($M = 2$) successfully detected the target over two choices of the three coupled channels. The MCF ($M = 3$) also successfully detected the target by employing all three channels.

The detection results for the MT are shown in Fig. 16. The Doppler frequency of the MT approximates to 2.5 Hz. The CC fails to detect the target over any of the three channels. By contrast, the MCF ($M = 2$) is capable of detecting the target over two choices of the three coupled channels, and the MCF ($M = 3$) has also successfully detected the target.

The above field test results demonstrate that compared to the conventional CC, the MCF can improve the quality of the range profile by performing joint detection over multiple channels. As a result, the MCF achieves superior detection performance when compared with the CC.

V. CONCLUSION

In this paper, a passive radar prototype using DVB-S as IO is developed for vehicle detection. A novel detection method called multichannel fusion (MCF) is proposed and implemented, which performs detection simultaneously over multiple orthogonal channels and makes decisions based on the weighted fusion of detection results from all the channels. Simulation results show that the proposed MCF achieves better performance than conventional single-channel-based cross-correlation (CC) detection under time varying interference that is i.i.d. across frequency channels and Doppler frequency shift caused by mobile vehicles. The multiple channel per carrier (MCPC) is also applied in the prototype to capture the signals from the multiple operating channels in parallel. Field test results further verify the superiority of the MCF over the CC and the novelty of the developed prototype.

The development of an upgraded prototype that realizes complete real-time detection by employing a processing unit with sufficient computing resources is planned for future work.

REFERENCES

[1] M. Tubaishat, P. Zhuang, Q. Qi, and Y. Shang, "Wireless sensor networks in intelligent transportation systems," *Wireless Commun. Mobile Comput.*, vol. 9, no. 3, pp. 287–302, Mar. 2009.

[2] S. Sivaraman and M. M. Trivedi, "Looking at vehicles on the road: A survey of vision-based vehicle detection, tracking, and behavior analysis," *IEEE Trans. Intell. Transp. Syst.*, vol. 14, no. 4, pp. 1773–1795, Dec. 2013.

[3] Q. Wang, J. Zheng, H. Xu, B. Xu, and R. Chen, "Roadside magnetic sensor system for vehicle detection in urban environments," *IEEE Trans. Intell. Transp. Syst.*, vol. 19, no. 5, pp. 1365–1374, May 2018.

[4] M. Malanowski, J. Misiurewicz, J. Kulpa, P. Samczynski, and K. Kulpa, "Analysis of detection range of FM-based passive radar," *IET Radar, Sonar Navigat.*, vol. 8, no. 2, pp. 153–159, Feb. 2014.

[5] D. K. P. Tan, H. Sun, Y. Lu, M. Lesturgie, and H. L. Chan, "Passive radar using Global System for Mobile communication signal: Theory, implementation and measurements," *IEE Proc.-Radar, Sonar Navigat.*, vol. 152, no. 3, pp. 116–123, Jun. 2005.

[6] P. Samczynski, K. Kulpa, M. Malanowski, P. Krysik, and L. Maslikowski, "A concept of GSM-based passive radar for vehicle traffic monitoring," in *Proc. Microw., Radar Remote Sens. Symp.*, Kiev, Ukraine, Aug. 2011, pp. 271–274.

[7] J. E. Palmer, H. A. Harms, S. J. Searle, and L. Davis, "DVB-T passive radar signal processing," *IEEE Trans. Signal Process.*, vol. 61, no. 8, pp. 2116–2126, Apr. 2013.

[8] A. Capria, D. Petri, M. Martorella, M. Conti, E. D. Mese, and F. Berizzi, "DVB-T passive radar for vehicles detection in urban environment," in *Proc. IEEE Int. Geosci. Remote Sens. Symp.*, Honolulu, HI, USA, Jul. 2010, pp. 3917–3920.

[9] P. Marques, A. Ferreira, F. Fortes, P. Sampaio, H. Rebelo, and L. Reis, "A pedagogical passive radar using DVB-S signals," in *Proc. 3rd Int. Asia–Pacific Conf. Synth. Aperture Radar (APSAR)*, Seoul, South Korea, Sep. 2011, pp. 1–4.

[10] Z. Sun, T. Wang, T. Jiang, C. Chen, and W. Chen, "Analysis of the properties of DVB-S signal for passive radar application," in *Proc. Int. Conf. Wireless Commun. Signal Process.*, Hangzhou, China, Oct. 2013, pp. 1–5.

[11] H. D. Griffiths and C. J. Baker, "Passive coherent location radar systems. Part 1: Performance prediction," *IEE-Proc. Radar, Sonar Navigat.*, vol. 152, no. 3, pp. 153–159, Jun. 2005.

[12] D. Cristallini, I. Pisciottano, and H. Kuschel, "Multi-band passive radar imaging using satellite illumination," in *Proc. Int. Conf. Radar (RADAR)*, Brisbane, QLD, Australia, Aug. 2018, pp. 1–6.

[13] S. Brisken, M. Moscadelli, V. Seidel, and C. Schwark, "Passive radar imaging using DVB-S2," in *Proc. IEEE Radar Conf. (RadarConf)*, Seattle, WA, USA, May 2017, pp. 0552–0556.

[14] I. Pisciottano, D. Cristallini, and D. Pastina, "Maritime target imaging via simultaneous DVB-T and DVB-S passive ISAR," *IET Radar, Sonar Navigat.*, vol. 13, no. 9, pp. 1479–1487, Sep. 2019.

[15] T. Tsao, M. Slamani, P. Varshney, D. Weiner, H. Schwarzlander, and S. Borek, "Ambiguity function for a bistatic radar," *IEEE Trans. Aerosp. Electron. Syst.*, vol. 33, no. 3, pp. 1041–1051, Jul. 1997.

[16] M. Malanowski and K. Kulpa, "Analysis of integration gain in passive radar," in *Proc. Int. Conf. Radar*, Adelaide, SA, Australia, Sep. 2008, pp. 323–328.

[17] T. Brenner, M. Klein, G. Weiss, and H. Kuschel, "Signals and data fusion in a deployable multiband passive-active radar (DMPAR)," in *Proc. IET Int. Conf. Radar Syst.*, Glasgow, U.K., Oct. 2012, pp. 1–6.

[18] M. Conti, F. Berizzi, M. Martorella, E. D. Mese, D. Petri, and A. Capria, "High range resolution multichannel DVB-T passive radar," *Int. J. Microw. Wireless Technol.*, vol. 4, no. 2, pp. 147–153, 2012.

[19] LyngSat. (Sep. 2019). *Apstar 6c at 134.0E.* [Online]. Available: https://www.lyngsat.com/Apstar-6C.html

[20] H. D. Griffiths, "Bistatic radar using satellite-borne illuminators," in *Proc. Int. Radar Conf.*, 2002, pp. 1–5.

[21] J. L. Garry, C. J. Baker, and G. E. Smith, "Evaluation of direct signal suppression for passive radar," *IEEE Trans. Geosci. Remote Sens.*, vol. 55, no. 7, pp. 3786–3799, Jul. 2017.

[22] O. Durmaz Incel and P. Jansen, "Characterization of multi-channel interference," in *Proc. 6th Intl Symp. Model. Optim.*, Berlin, Germany, 2008, pp. 429–435.

[23] M. Albu and G. T. Heydt, "On the use of rms values in power quality assessment," *IEEE Trans. Power Del.*, vol. 18, no. 4, pp. 1586–1587, Oct. 2003.

[24] J. G. Proakis and D. G. Manolakis, *Digital Signal Processing: Principles, Algorithms, and Applications*, 3rd ed. Upper Saddle River, NJ, USA: Prentice-Hall, 1996.

[25] H.-Y. Zhao, J. Liu, Z.-J. Zhang, H. Liu, and S. Zhou, "Linear fusion for target detection in passive multistatic radar," *Signal Process.*, vol. 130, pp. 175–182, Jan. 2017.

[26] Q. Chen, J. Li, J. Zhu, C. Song, and Z. Xu, "A multi-channel based passive detection strategy for high-speed moving target in the airspace under varying interference," in *Proc. 23rd Asia–Pacific Conf. Commun. (APCC)*, Perth, WA, Australia, Dec. 2017, pp. 1–5.

[27] E. Etsi, "Digital video broadcasting (DVB); Framing structure, channel 673 coding and modulation for 11/12 GHz satellite service," Eur. Telecommun. Standards Inst., Sophia Antipolis, France, Tech. Rep. ETSI 674 EN-300-421-v1.1.2, 1997.

[28] M. A. Richards, *Fundamentals Radar Signal Processing*. New York, NY, USA: McGraw-Hill, 2005.
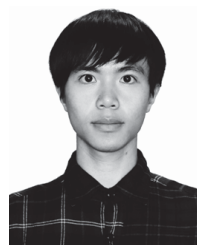
JUNJIE LI (Graduate Student Member, IEEE) was born in Guangdong, China, in 1993. He received the B.S. degree in naval architecture and marine engineering from Dalian Maritime University, in 2016. He is currently pursuing the Ph.D. degree in marine information science and engineering with Zhejiang University. His research interests include passive radar and millimeter wave radar signal processing.

JUNKANG WEI (Graduate Student Member, IEEE) was born in Hebi, Henan, China, in 1995. He received the B.S. degree in marine electronics and electrical engineering from Dalian Maritime University, in 2018. He is currently pursuing the M.S. degree in marine electronic information engineering with Zhejiang University. His research interest includes passive radar systems.

ZHIHUI CAO (Graduate Student Member, IEEE) was born in Jiujiang, Jiangxi, China, in 1996. He received the B.S. degree in measurement and control technology and instrumentation from Hangzhou Dianzi University, in 2018. He is currently pursuing the Ph.D. degree in marine technology and engineering with Zhejiang University. His research interests include passive radar and millimeter wave radar signal processing.

QIN CHEN (Graduate Student Member, IEEE) was born in Hunan, China, in 1994. He received the B.S. degree in marine engineering and technology from Zhejiang University, China, in 2012, where he is currently pursuing the M.S. degree with the Ocean College. His current research interests include the radar target detection, multisensor position calibration, and marine satellite communication.

LIJIE YANG was born in Zhejiang, China, in 1991. He received the B.S. and Ph.D. degrees in electronic and information engineering from Zhejiang University, Hangzhou, China, in 2013 and 2019, respectively. He is currently an Assistant Researcher with the Zhejiang Lab. His current research interests include the design of mm-wave radar systems, radar calibration technology, and mm-wave transceiver circuits.

CHUNYI SONG (Member, IEEE) received the Ph.D. degree in electronic and communication engineering from Waseda University, Tokyo, Japan. He was a Research Associate with Waseda University, from 2007 to 2009. Then, he joined the National Institute of Information and Communications Technology (NICT), Japan, as a Researcher, from 2009 to 2013, and as a Senior Researcher, in 2014. Since 2014, he has been with Zhejiang University, China, as an Associate Professor, where he is also serving as the Vice Director of the Key Laboratory of Ocean Observation-Imaging Testbed of Zhejiang Province. He was elected to Thousand Talents Program of Zhejiang Province, in 2016, and a Core Member of Leading Innovative Team of Zhejiang, in 2018.

ZHIWEI XU (Senior Member, IEEE) received the Ph.D. degree in integrated circuits and systems from the University of California at Los Angeles, in 2003. He held senior manager positions with G-Plus Inc., SST Communications, Conexant Systems, and NXP Semiconductors Inc., before he joining HRL Laboratories, where he led development for wireless LAN and SoC solutions for proprietary wireless multimedia systems, CMOS cellular transceiver, multimedia over cable (MoCA) system, and TV tuners. He is currently with Zhejiang University, as a Professor, working on cognitive radios, high-speed ADC, and mmWave ICs. He has authored/coauthored 70 publications, one contribution to the encyclopedia of wireless and mobile communications, ten granted patents, and over 20 pending patents. He was elected to China's Thousand Talents Program, in 2014, and a Team Leader of Leading Innovative Team of Zhejiang, in 2018. He serves as the technical program committee for international workshop on mm-wave communications: from circuit to network and as a Series Editor for the *IEEE Communications Magazine*.

• • •